Multi-State Epoxidation of Ethene by Cytochrome P450: A Quantum Chemical Study

Sam P. de Visser, François Ogliaro, Nathan Harris, and Sason Shaik*

Contribution from the Department of Organic Chemistry and the Lise Meitner-Minerva Center for Computational Quantum Chemistry, The Hebrew University of Jerusalem, 91904 Jerusalem, Israel

Received September 29, 2000. Revised Manuscript Received January 11, 2001

Abstract: The epoxidation of ethene by a model for Compound I of cytochrome P450, studied by the use of density functional B3LYP calculations, involves two-state reactivity (TSR) with multiple electromer species, hence "multi-state epoxidation". The reaction is found to proceed in stepwise and effectively concerted manners. Several reactive states are involved; the reactant is an (oxo)iron(IV) porphyrin cation radical complex with two closely lying spin states (quartet and doublet), both of which react with ethene to form intermediate complexes with a covalent C−O bond and a carbon-centered radical (radical intermediates). The radical intermediates exist in two electromers that differ in the oxidation state of iron; $Por^{+\bullet}Fe^{III}OCH_2CH_2^{\bullet}$ and $PorFe^{IV}$-$OCH_2CH_2^{\bullet}$ (Por = porphyrin). These radical intermediates exist in both the doublet- and quartet spin states. The quartet spin intermediates have substantial barriers for transformation to the quartet spin $PorFe^{III}$−epoxide complex (2.3 kcal mol^{-1} for $PorFe^{IV}OCH_2CH_2^{\bullet}$ and 7.2 kcal mol^{-1} for $Por^{+\bullet}Fe^{III}OCH_2CH_2^{\bullet}$). In contrast, the doublet spin radicals collapse to the corresponding $PorFe^{III}$−epoxide complex with virtually no barriers. Consequently, the lifetimes of the radical intermediates are much longer on the quartet- than on the doublet spin surface. The loss of isomeric identity in the epoxide and rearrangements to other products arise therefore mostly, if not only, from the quartet process, while the doublet state epoxidation is effectively concerted (Scheme 7). Experimental trends are discussed in the light of the computed mechanistic scheme, and a comparison is made with closely related mechanistic schemes deduced from experiment.

1. Introduction

Cytochrome P450 enzymes (P450) are the most important members of the heme-thiolate proteins family, all containing in their active site an iron porphyrin which is linked to the protein by an iron−cysteinate bond.[1−8] P450s are present in most organisms (mammals, fish, invertebrates, plants, and microorganisms), and they catalyze a large variety of reactions, such as oxidation, reduction, isomerization, and dehydration. These reactions are important for the biodegradation of toxic substances, as well as for biosynthesis (of sex hormones for example). As such, P450 enzymes are vital, drawing a soaring interest aimed at the understanding of their nature and reactivity patterns. Many experimental investigations have been performed on cytochrome P450 and related enzymes. Important insights into the nature of the enzymatic processes resulted from studies of various isozymes as well as of synthetic model metalloporphyrins in different oxidation states and with various ligands.[9−29] The most extensive research efforts were devoted to the

* Author to whom correspondence should be addressed. Fax: +972-2-6585345. E-mail: sason@yfaat.ch.huji.ac.il.

(1) Ostovic, D.; Bruice, T. C. *Acc. Chem. Res.* **1992**, *25*, 314.
(2) Meunier, B. *Chem. Rev.* **1992**, *92*, 1411.
(3) Groves, J. T.; Han, Y.-Z. In *Cytochrome P450: Structure, Mechanism and Biochemistry*, 2nd ed.; Ortiz de Montellano, P. R., Ed.; Plenum Press: New York, 1995; p 3.
(4) Woggon, W.-D. *Top. Curr. Chem.* **1996**, *184*, 40.
(5) Sono, M.; Roach, M. P.; Coulter, E. D.; Dawson, J. H. *Chem. Rev.* **1996**, *96*, 2841.
(6) Ortiz de Montellano, P. R. *Acc. Chem. Res.* **1998**, *31*, 543.
(7) Newcomb, M.; Toy, P. H. *Acc. Chem. Res.* **2000**, *33*, 449.
(8) Kadish, K. M., Smith, K. M., Guilard, R., Eds. *The Porphyrin Handbook*; Academic Press: San Diego, 2000. In particular the following Chapters: (a) Mansuy, D.; Battioni, P. Chapter 26, Vol. 4, p 1. (b) Groves, J. T.; Shalyaev, K.; Lee, J. Chapter 27, Vol. 4, p 17. (c) Suslick, K. S. Chapter 28, Vol. 4, p 41. (d) Watanabe Y. Chapter 30, Vol. 4, p 97. (e) Meunier, B.; Robert, A.; Pratviel, G.; Bernadou, J. Chapter 31, Vol. 4, p 119.
(9) Groves, J. T. *J. Chem. Educ.* **1985**, *62*, 928.
(10) Dawson, J. H. *Science* **1988**, *240*, 433.
(11) Gross, Z.; Nimri, S.; Simkhovich, L. *J. Mol. Catal. A: Chem.* **1996**, *113*, 231.
(12) Goldfarb, D.; Bernardo, M.; Thomann, H.; Kroneck, P. M. H.; Ullrich, V. *J. Am. Chem. Soc.* **1996**, *118*, 2686.
(13) Toy, P. H.; Dhanabalasingam, B.; Newcomb, M.; Hanna, I. H.; Hollenberg, P. F. *J. Org. Chem.* **1997**, *62*, 9114.
(14) Wertz, D. L.; Sisemore, M. F.; Selke, M.; Driscoll, J.; Valentine, J. S. *J. Am. Chem. Soc.* **1998**, *120*, 5331.
(15) Toy, P. H.; Newcomb, M.; Hollenberg, P. F. *J. Am. Chem. Soc.* **1998**, *120*, 7719.
(16) Hart-Davis, J.; Battioni, P.; Boucher, J.-L.; Mansuy, D. *J. Am. Chem. Soc.* **1998**, *120*, 12524.
(17) Newcomb, M.; Shen, R.; Choi, S.-Y.; Toy, P. H.; Hollenberg, P. F.; Vaz, A. D. N.; Coon, M. J. *J. Am. Chem. Soc.* **2000**, *122*, 2677.
(18) Schlichting, I.; Berendzen, J.; Chu, K.; Stock, A. M.; Maves, S. A.; Benson, D. E.; Sweet, R. M.; Ringe, D.; Petsko, G. A.; Sligar, S. G. *Science* **2000**, *287*, 1615.
(19) Collman, J. P.; Hampton, P. D.; Brauman, J. I. *J. Am. Chem. Soc.* **1990**, *112*, 2977.
(20) Gross, Z.; Nimri, S. *Inorg. Chem.* **1994**, *33*, 1731.
(21) Groves, J. T.; Gross, Z.; Stern, M. K. *Inorg. Chem.* **1994**, *33*, 5065.
(22) Gross, Z.; Nimri, S. *J. Am. Chem. Soc.* **1995**, *117*, 8021.
(23) Czarnecki, K.; Nimri, S.; Gross, Z.; Proniewicz, L. M.; Kincaid, J. R. *J. Am. Chem. Soc.* **1996**, *118*, 2929.
(24) Vaz, A. D. N.; McGinnity, D. F.; Coon, M. J. *Proc. Natl. Acad. Sci. U.S.A.* **1998**, *95*, 3555.
(25) Yang, S. J.; Nam, W. *Inorg. Chem.* **1998**, *37*, 606.
(26) Mayhew, M. P.; Reipa, V.; Holden, M. J.; Vilker, V. L. *Biotechnol. Prog.* **2000**, *16*, 610.
(27) Nam, W.; Lim, M. H.; Lee, H. J.; Kim, C. *J. Am. Chem. Soc.* **2000**, *122*, 6641.
(28) Adam, W.; Stegmann, V. R.; Saha-Möller, C. R. *J. Am. Chem. Soc.* **1999**, *121*, 1879.
(29) Gross, Z.; Nimri, S.; Barzilay, C. M.; Simkhovich, L. *J. Biol. Inorg. Chem.* **1997**, *2*, 492.

10.1021/ja003544+ CCC: $20.00
Published on Web 03/13/2001

Scheme 1

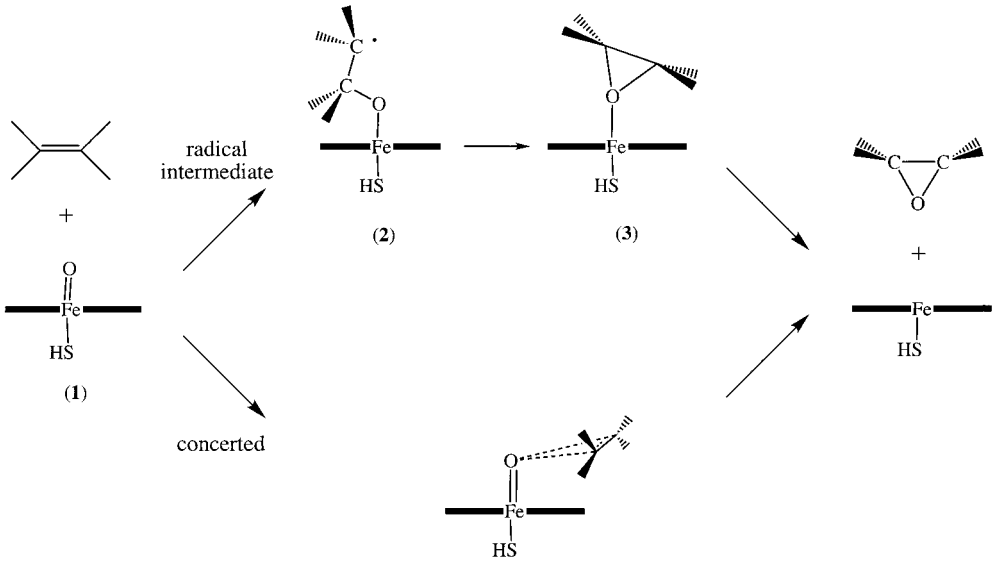

hydroxylation of alkanes and the epoxidation of alkenes.[1−5,19−29] In a most recent paper[30] we addressed the problems and controversies which surround the alkane hydroxylation mechanism. The present paper completes the description of these mechanistic twins and presents a density functional investigation of ethene epoxidation, Scheme 1.

An important mechanistic issue in P450 oxidations is the possible participation of two or more oxidizing intermediates.[17,21,27] The number of mechanistic possibilities for the two (or three) oxidants is not small, and the treatment of the entire problem by computational means is beyond the scope of a single paper. Since it is generally accepted that the primary oxidative form of the catalyst is an (oxo)iron(IV) species (**1** in Scheme 1), we have restricted ourselves to this structure as the starting point for the calculations. The electronic structure of **1** has been amply discussed in the literature by several groups.[31−33] The analogous species in heme peroxidases has been treated by Kuramochi et al.[34] and the Siegbahn group.[35−38] Other iron porphyrin systems have been studied by Parrinello et al.,[39] while manganese oxenes have been addressed by Ghosh and Gonzalez.[40]

Our past studies[30,41−46] of the hydroxylation mechanism have shown that major controversies could be explained with a two-state reactivity (TSR) model. In short, it was demonstrated that two closely lying electronic states of **1**, the doublet ($S = {}^1/_2$) and quartet ($S = {}^3/_2$) spin state, compete and are jointly responsible for the reaction mechanism of hydroxylation. The epoxidation of ethene by Mn(salen) has been computed by Linde et al. and shown to involve crossing of a triplet ground state and an initially high-lying quintet state, en route to product formation.[47] However, to the best of our knowledge, the complete epoxidation mechanism by the iron oxene species of P450 has never been studied before. The present paper addresses the mechanistic questions of alkene epoxidation by P450, concentrating on the elementary steps that lead from the interaction of **1** with olefins eventually to the epoxide product complex, **3**. This was done by studying a model reaction in which the cysteinato ligand in the ferryl oxene (**1**) oxidant is simplified by SH^- (a few critical species were ascertained for CH_3S^-), the porphyrin is devoid of side-chains, and ethene serves as the olefin. This model system will serve to reveal general tendencies.

Since previous attempts to compute a concerted oxygen insertion by iron oxene,[48] dioxygen,[49] and manganese oxene species[47] revealed that this is a high-energy pathway, we focus here on the end-on attack in Scheme 1. Indeed, there is a growing recognition[29] that the reactions of **1** with olefins are stepwise, that is, the carbon−oxygen bonds of the epoxide are formed in two consecutive steps. An initial intermediate is produced after formation of a single C−O bond, followed by ring closure to produce the epoxide. Of the three proposed intermediates— metallocycle, cationic, and radical—the latter is more strongly indicated by experimental results. In principle, two forms of the radical intermediate are possible;[21,29] iron(IV) ligated by a closed-shell porphyrin versus iron(III) porphyrin cation radical (possible equilibration of the intermediates have also been considered).[20−22,29] As our present study shall reveal, there is an interplay of an effectively concerted low-spin mechanism and a stepwise high-spin one with observable radical

(30) Ogliaro, F.; Harris, N.; Cohen, S.; Filatov, M.; de Visser, S. P.; Shaik, S. *J. Am. Chem. Soc.* **2000**, *122*, 8977.
(31) Harris, D. L.; Loew, G. H. *J. Am. Chem. Soc.* **1998**, *120*, 8941.
(32) Loew, G. H.; Harris, D. L. *Chem. Rev.* **2000**, *100*, 407.
(33) Green, M. T. *J. Am. Chem. Soc.* **1999**, *121*, 7939.
(34) Kuramochi, H.; Noodleman, L.; Case, D. A. *J. Am. Chem. Soc.* **1997**, *119*, 11442.
(35) Siegbahn, P. E. M.; Crabtree, R. H. *J. Am. Chem. Soc.* **1997**, *119*, 3103.
(36) Wirstam, M.; Blomberg, M. R. A.; Siegbahn, P. E. M. *J. Am. Chem. Soc.* **1999**, *121*, 10178.
(37) Siegbahn, P. E. M.; Blomberg, M. R. A. *Annu. Rev. Phys. Chem.* **1999**, *50*, 221.
(38) Siegbahn, P. E. M.; Blomberg, M. R. A. *Chem. Rev.* **2000**, *100*, 421.
(39) (a) Rovira, C.; Kunc, K.; Hutter, J.; Ballone, P.; Parrinello, M. *J. Phys. Chem. A* **1997**, *101*, 8914. (b) Rovira, C.; Parrinello, M. *Int. J. Quantum Chem.* **1998**, *70*, 387.
(40) Ghosh, A.; Gonzalez, E. *Isr. J. Chem.* **2000**, *40*, 1.
(41) Shaik, S.; Filatov, M.; Schröder, D.; Schwarz, H. *Chem. Eur. J.* **1998**, *4*, 193.
(42) Filatov, M.; Harris, N.; Shaik, S. *J. Chem. Soc., Perkin Trans. 2* **1999**, 399.
(43) Filatov, M.; Harris, N.; Shaik, S. *Angew. Chem., Int. Ed.* **1999**, *38*, 3510.
(44) Schröder, D.; Shaik, S.; Schwarz, H. *Acc. Chem. Res.* **2000**, *33*, 139.
(45) Harris, N.; Cohen, S.; Filatov, M.; Ogliaro, F.; Shaik, S. *Angew. Chem., Int Ed.* **2000**, *39*, 2003.
(46) Ogliaro, F.; Cohen, S.; Filatov, M.; Harris, N.; Shaik, S. *Angew. Chem., Int. Ed.* **2000**, *39*, 3851.
(47) Linde, C.; Åkermark, B.; Norrby, P.-O.; Svensson, M. *J. Am. Chem. Soc.* **1999**, *121*, 5083.
(48) Filatov, M.; Shaik, S. *J. Phys. Chem. A* **1998**, *102*, 3835.
(49) Filatov, M.; Reckien, W.; Peyerimhoff, S. D.; Shaik, S. *J. Phys. Chem. A*, **2000**, *104*, 12014.

Scheme 2

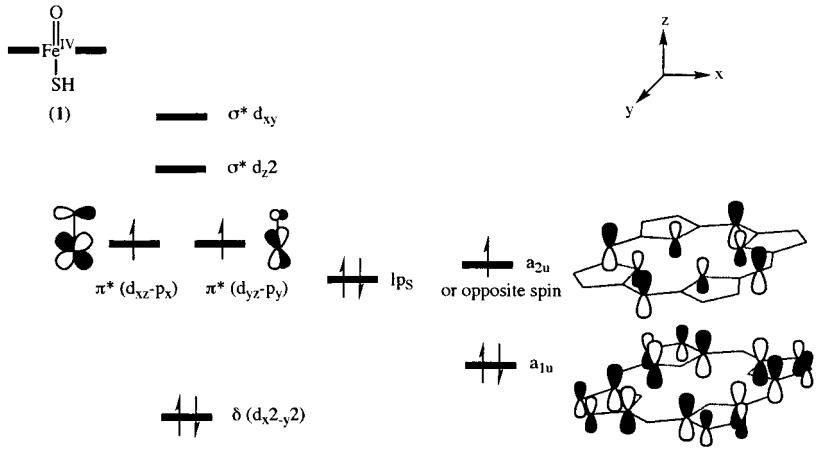

intermediates on the reaction pathway. Furthermore, our analysis exposes four such intermediates, which differ in their electronic configurations and have significantly different lifetimes. Several puzzling experimental observations, such as occasional *cis*/*trans* isomerization,[21] sensitivity of the reaction to the olefin's donor capability,[8,50] and production of aldehydes[8,21,29] might be accounted for by the computed reaction pathways.

2. Methods

The mechanism of epoxidation of ethene by P450 was studied using the Jaguar 4.0 program package.[51] Calculations were performed using the B3LYP hybrid density functional method[52−55] in combination with the Los Alamos effective core potential coupled with the double-ζ LACVP basis set[56,57] for iron and an all-electron 6-31G basis set for the rest of the atoms; hence, LACVP/6-31G. Previous calculations from our group[30,41−46] showed that these type of basis sets are sufficient to get qualitatively reliable results. Single-point calculations using the polarized LACVP*/6-31G* basis set on the different TS1 structures gave energy differences of 1.2 kcal mol^{-1} between ^{4}**TS1-IV** and ^{2}**TS1-IV** and of 4.5 kcal mol^{-1} between ^{4}**TS1-IV** and ^{2}**TS1-III′**, compared with 1.0 and 4.9 kcal mol^{-1} with the LACVP/6-31G basis set, vide supra.

Version 4.0 of the Jaguar program package contains restricted open shell DFT (RODFT) and unrestricted DFT (UDFT) methods. As the studies presented here concern a doublet spin state with three unpaired electrons (vide infra), the main calculations on the quartet and doublet spin state presented here were performed using the UDFT method. In addition to this, some exploratory calculations on the quartet- and sextet spin potential energy surfaces were done using the RODFT method. It was found that the iron porphyrin reactants were 17.0 kcal mol^{-1} higher in energy in the sextet state (δ $d_{x^2-y^2}$ → σ* d_{xy} excitation) than in the quartet state. Similarly, the sextet radical complex (**2**) was 17.1 kcal mol^{-1} higher in energy than the corresponding quartet spin state. The sextet product (^{6}**3**) was 1.5 kcal mol^{-1} higher than the quartet ^{4}**3**. Consequently, the sextet state corresponds to a highly excited state, and therefore the potential energy surface of this state was not explored further.

The coordinating cysteinato group in **1** was described by a sulfide group. To ascertain that the mechanism is qualitatively invariant to the choice of ligand, we characterized also the intermediates ^{4}**2** for SCH_3^-. In any event, SH^- should be considered as a model ligand designed to reveal the qualitative nature of the mechanism. All structures were fully optimized followed by a complete numerical frequency analyses for the doublet and quartet spin states.

Transition states were located by tracing a potential energy scan along a choice reaction coordinate, using tight steps, with full optimization of the rest of the geometrical degrees of freedom. In the case of **TS1** which leads to C−O bond formation, the reaction coordinate parameter was the C−O bond length. In the case of **TS2** which leads to ring-closure this was the C−C−O angle (see below for details). Subsequently, at the point of maximum energy along each of these reaction coordinates, a full transition-state geometry optimization was carried out in which all parameters were optimized. A complete frequency analysis was performed for all of the transition states.

Although all calculations performed here were run without symmetry constraints, the optimized species are close to being C_s symmetry. The mirror plane in C_s symmetry passes through the S−Fe−O−C atoms. As a result the *x* and *y* axes of the coordinate system do not pass through the nitrogen atoms of the porphyrin ring but midway between those. A d-block diagram used often in the literature[8,29] involves a coordinate system where the *x* and *y* axes pass through the nitrogen atoms of the porphyrin ring. This diagram, however, switches the labels of the $d_{x^2-y^2}$ and d_{xy} orbitals relative to their ordering in Scheme 2 (vide infra). Recall, however, that in any coordinate system, the lowest orbital is δ-type followed by two π-types. The higher-lying orbitals are σ*-types, one (d_{z^2}) along the *z* axis and the other (either d_{xy} or $d_{x^2-y^2}$ depending on the coordinate system) in the porphyrin plane. See refs 42 and 43 for details.

3. Results

To elucidate the complex behavior of the reaction process, one needs to understand the electronic states involved. Therefore, we will start the section with a detailed description of the essential molecular orbitals and their change of occupation during the oxidation reaction.

3.1. Key Orbitals Involved in the Process. The ordering of the highest occupied and lowest virtual d-type orbitals of reactant Fe(Por)OSH (**1**) are depicted in Scheme 2. The 3d atomic orbitals of the iron atom form bonding and antibonding combinations with the oxygen and sulfur atomic orbitals. The highest doubly occupied orbital of those is the δ-type $d_{x^2-y^2}$ orbital. A degenerate pair of singly occupied π* orbitals are made up from the antibonding combinations of the oxygen $2p_x$ ($2p_y$) with the iron $3d_{xz}$ ($3d_{yz}$) atomic orbitals. Two virtual orbitals are the d_{z^2} and d_{xy} antibonding orbitals. The d_{z^2} orbital has antibonding character along the O−Fe−S axis, while d_{xy} is antibonding in the in-plane Fe−N linkages. With this d-block

(50) Groves, J. T.; Nemo, T. E. *J. Am. Chem. Soc.* **1983**, *105*, 5786.
(51) *Jaguar 4.0*; Schrödinger, Inc.: Portland, Oregon, 1998.
(52) Becke, A. D. *J. Chem. Phys.* **1992**, *96*, 2155.
(53) Becke, A. D. *J. Chem. Phys.* **1992**, *97*, 9173.
(54) Becke, A. D. *J. Chem. Phys.* **1993**, *98*, 5648.
(55) Lee, C.; Yang, W.; Parr, R. G. *Phys. Rev. B* **1988**, *37*, 785.
(56) Hay, J. P.; Wadt, W. R. *J. Chem. Phys.* **1985**, *82*, 99.
(57) Friesner, R. A.; Murphy, R. B.; Beachy, M. D.; Ringlanda, M. N.; Pollard, W. T.; Dunietz, B. D.; Cao, Y. X. *J. Phys. Chem. A* **1999**, *103*, 1913.

Scheme 3

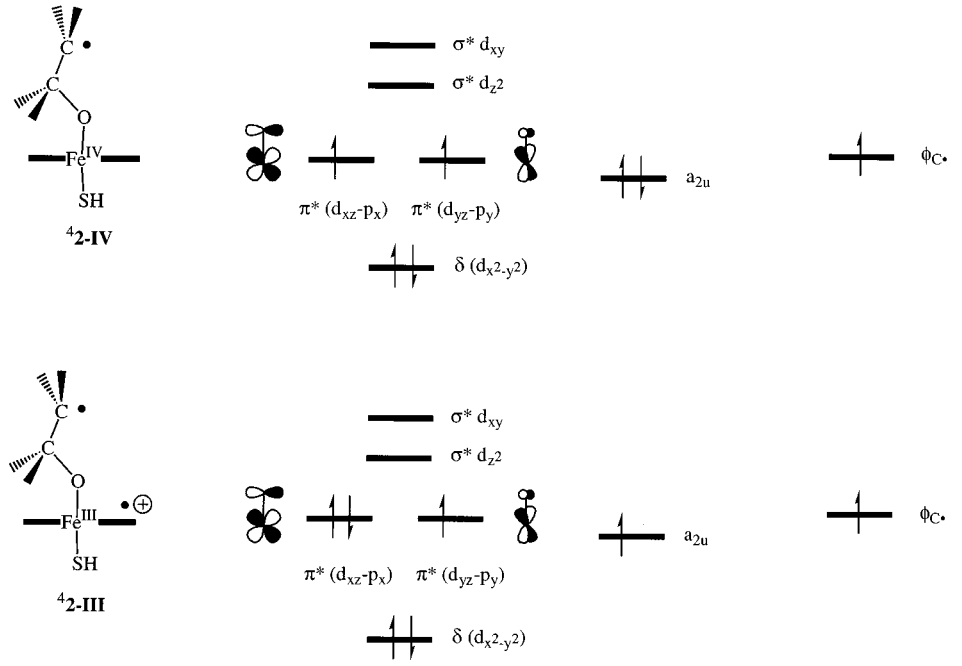

filling the iron atom is in the Fe^{IV} oxidation state. Other high-lying occupied orbitals are a lone-pair orbital located on the sulfur atom (lp_S) and two porphyrin orbitals. The latter two orbitals are designated a_{1u} and a_{2u} following the assignment from the literature.[30,41−45] *It must be remembered, though, that the a_{2u} orbital has a mixed porphyrin−thiolate character[30], and it is through this mixed character that axial ligands differ from each other (e.g., imidazole ligands mix less than thiolate[42])*. For simplicity, we show a pure a_{2u} orbital.

It was shown[30−33,41−46] that the ground state of **1** has three unpaired electrons, two on iron and one on the porphyrin ring, located in the $\pi^*(d_{xz}-p_x)$, $\pi^*(d_{yz}-p_y)$ and a_{2u} orbitals. The π^* electrons must maintain a triplet-relation, that is both with alpha spin, while the a_{2u} orbital in **1** has a spin-up electron in the quartet state and a spin-down electron in the doublet state. The quartet- and doublet states are frequently referred to as ferro- and antiferromagnetically coupled systems.[8] Since the π^* and a_{2u} orbitals are disjoined, the interaction between the two π^* electrons and the single a_{2u} electron is minimal. Hence, the calculated LACVP/6-31G energy gap between the quartet- and doublet states is only 0.1 kcal mol^{-1}. The LACVP*/6-31G* energy gap is only −0.05 kcal mol^{-1} in favor of the doublet spin state. Similar results were obtained with larger basis sets up to 6-311+G*.[46] It is this proximity of the two states which is responsible for the two-state-reactivity feature of the mechanism. The same state proximity was noted for SCH_3^- and cysteinate as ligands,[46] as well as for nitrogen ligands.[42]

In all calculations presented here, the lp_S and a_{1u} orbitals are doubly occupied. It was shown in one of our previous papers[30,46] that excitation from the lone pair orbital lp_S to a_{2u} leads to an excited state 6−8 kcal mol^{-1} higher than the electronic state with a singly occupied a_{2u} orbital. Similarly, the transition states for C−H bond activation by these sulfur-radical states were found to be higher in energy.[30] Thus, epoxidation originating from these sulfur radical states was not studied.

When an ethene molecule approaches **1**, a covalent bond can be formed between the oxygen atom and one of the carbon atoms of the ethene moiety, leading to a radical center on the terminal carbon atom (Scheme 1). One of the electrons initially in the π-bond of the ethene moiety is formally donated into one of the singly occupied orbitals of the iron oxene **1**, as shown in Scheme 3. For simplicity, only the quartet state situations are presented in Scheme 3 (the lone pair orbital on sulfur (lp_S) and a_{1u} remain doubly occupied and are therefore omitted). The diagram on top shows the situation whereby the a_{2u} orbital is filled (the porphyrin cation radical is reduced), while the bottom diagram corresponds to the situation in which one of the π^* orbitals of iron accepts the electron (the metal is reduced). Filling the a_{2u} orbital retains the oxidation state of iron at Fe-IV, while an Fe-III oxidation state is created when the electron is transferred to a π^* d-orbital. In addition to the orbital dichotomy, with the C-radical included each complex still can be in either a doublet or a quartet spin state. Consequently, five possible states for radical complex **2** are of importance, that is quartet spin with Fe-IV (^{4}**2-IV**), quartet spin with Fe-III (^{4}**2-III**), doublet spin with Fe-IV (^{2}**2-IV**), and doublet spin with Fe-III (^{2}**2-III** and ^{2}**2-III′**). The π^* electrons in the Fe^{IV} electromer strongly prefer to remain in high spin arrangement. Consequently, the low-lying doublet ^{2}**2-IV** intermediate will possess a spin-down electron in $\phi_{C\bullet}$. On the other hand, the a_{2u}, π^*, and $\phi_{C\bullet}$ electrons of Fe^{III} electromer are all weakly coupled and lead therefore to two nearly degenerate doublet-state situations, drawn in Scheme 4 using only essential orbitals. The calculations show that the ^{2}**2-III** intermediate is lower by 1.7 kcal mol^{-1} than ^{2}**2-III′**.

Following the O−C bond formation there occurs ring-closure to form the iron-epoxide complex **3**. The orbital occupations of the doublet- and quartet states of the product complex **3** are depicted in Scheme 5 (recall, the sextet state is higher-lying and anyway does not play a role up to this stage). Only essential orbitals are drawn in Scheme 5. Starting from ^{4}**2-IV** (Scheme 3), an electron is formally transferred from the $\phi_{C\bullet}$ orbital to the d_{z^2} orbital,[30] leading to an iron(III)-epoxide complex in a quartet spin state in Scheme 5. The reaction path via the Fe-III radical complex, however, requires a double excitation of an alpha spin electron from the $\phi_{C\bullet}$ orbital to the d_{z^2} orbital and of a beta spin electron from $\pi^*(d_{xz} - p_x)$ to the a_{2u} orbital. Thus, already at this stage of the analysis we expected that the barrier for ring-closure will be higher for ^{4}**2-III** than for ^{4}**2-IV** (vide

Scheme 4

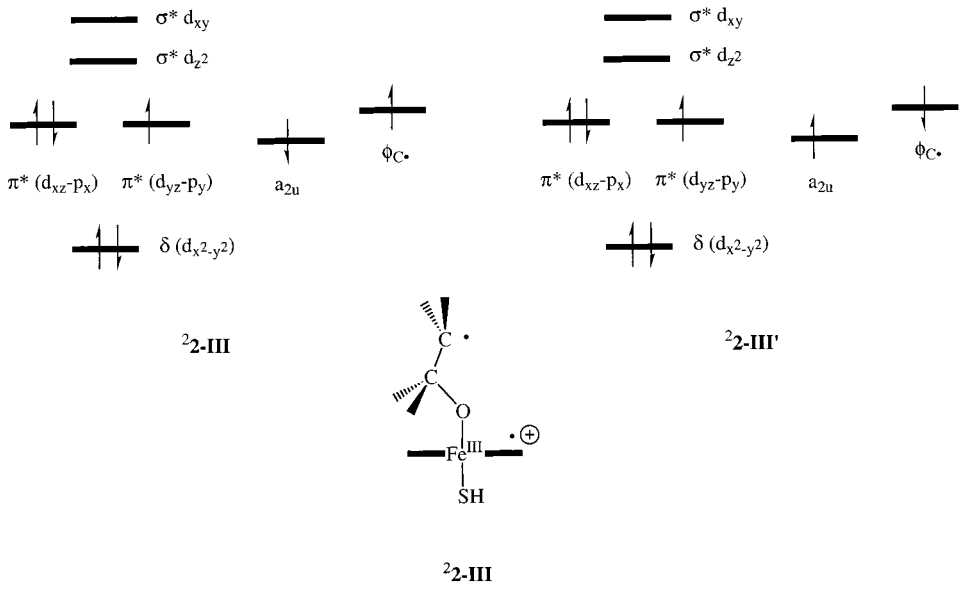

Scheme 5

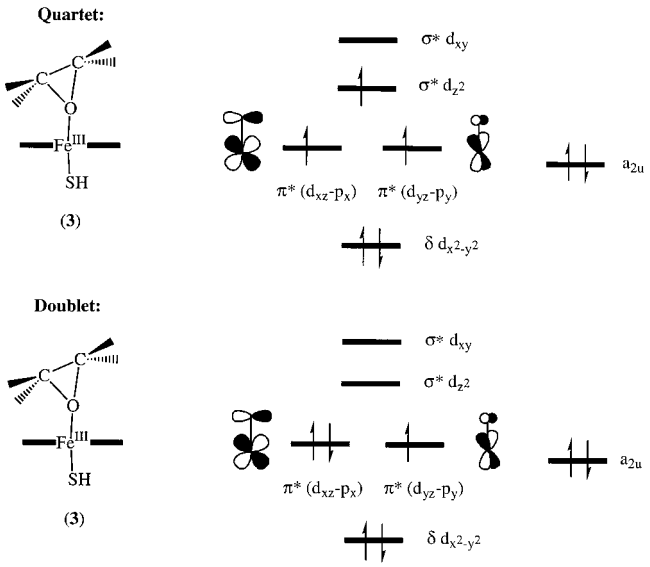

infra). In the doublet state, the electron from $\phi_{C\bullet}$ is transferred to $\pi^*(d_{xz} - p_x)$ in the case of the ^{2}**2-IV** electromer, and to the a_{2u} orbital in the case of the ^{2}**2-III** and ^{2}**2-III′** electromers. It follows that, on the doublet surface the three electromers of **2** will possess lower barriers for ring-closure than on the quartet surface.

3.2. Geometries. Optimized geometries of the complexes **2** and **3** in the lowest doublet- and quartet spin states are schematically depicted in Figure 1. Relative energies and group spin densities are collected in Table 1. Absolute energies and group charges can be found in Table A of the Supporting Information. All five electronic states in Figure 1 correspond to minimum energy structures having only real frequencies.

Geometrically, the doublet- and quartet states of **2-IV** closely resemble each other. Similarly, the doublet- and quartet states of **2-III** are basically alike. In the case of the **2-IV** structures, the epoxide moiety is in a plane almost orthogonal to the porphyrin ring bisecting the plane between the four nitrogen atoms. The **2-III** (**2-III′**) structures, however, have an Fe−O−C−C dihedral of 171.0° (quartet) and 174.9° (−176.0°) (doublet), while the **2-IV** structures have a dihedral of 178.8° (quartet) and 179.1° (doublet). Furthermore, the **2-III** isomers have smaller Fe−O−C angles compared with those of the **2-IV** entities. In agreement with our previous calculations[43] the iron-III complex has longer Fe−S and Fe−O bonds than the corresponding Fe-IV complex. In particular, the quartet state has a substantially shorter Fe−S bond length of 2.381 Å in ^{4}**2-IV** with respect to the 2.447 Å in ^{4}**2-III**. The intermediate states, ^{4}**2-IV** and ^{4}**2-III** were characterized also for SCH_3^- as a ligand, and gave a very similar picture. Thus, ^{4}**2-IV** lies 1.2 kcal mol^{-1} above the reactant state (compared with 0.6 kcal mol^{-1} for SH^-), whereas the ^{4}**2-III** intermediate lies 2.0 kcal mol^{-1} above the reactant state (compared with 3.2 kcal mol^{-1} for SH^-).

The product complex **3** in Figure 1 has a long Fe−O bond length of 2.555 Å in the quartet state and a shorter one of 2.172 Å in the doublet state. The long bond in the quartet is the result of filling the $\sigma^*(d_{z^2})$ orbital with one electron, in comparison with the doublet state in which the electron adds to a π^* d-orbital. In addition, ^{4}**3** has an Fe−S bond distance of 2.497 Å, whereas the doublet state has a bond length of only 2.294 Å, for precisely the same reasons as given for the respective Fe−O bonds, and in accord with the corresponding methanol complexes.[30] A complex of Ru^{II} with epoxides was described

Table 1. Relative Energies (kcal mol^{-1}) and Group Spin Densities (ρ) of Optimized Structures

	relative energy	ρ_{Fe}	ρ_{Por}	ρ_O	ρ_{SH}	ρ_{CH_2}	ρ_{CH_2}[e]
^{4}**1**[a]	0.0 (0.0)[d]	1.0	0.4	1.0	0.6	0.0	0.0
^{4}**1a**[b]	−0.2	1.0	0.4	1.0	0.6	0.0	0.0
^{4}**TS1-IV**	+13.9	1.3	0.1	0.8	0.3	−0.1	0.6
^{4}**2-IV**	+0.6 (1.2)[d]	1.9	−0.1	0.3	0.0	0.0	0.9
^{4}**2-III**	+3.2 (2.0)[d]	0.9	0.4	0.3	0.4	0.0	1.0
^{4}**TS2-IV**	+2.9	2.3	−0.1	−0.1	0.3	0.0	0.6
^{4}**TS2-III**[c]	+10.4	1.6	0.2	0.0	0.5	−0.1	0.8
^{4}**3**	−25.5	2.6	0.0	0.0	0.4	0.0	0.0
^{2}**1**[a]	+0.1 (0.03)[d]	1.2	−0.5	0.9	−0.6	0.0	0.0
^{2}**1a**[b]	−0.2	1.2	−0.5	0.9	−0.6	0.0	0.0
^{2}**TS1-IV**	+14.9	1.8	−0.3	0.2	−0.4	0.1	−0.4
^{2}**2-IV**	+0.9	2.0	−0.1	0.3	−0.3	0.1	−1.0
^{2}**2-III**	+1.4	1.2	−0.5	−0.1	−0.4	0.0	0.8
^{2}**2-III′**	+3.1	0.8	0.4	0.2	0.4	0.1	−0.9
^{2}**3**	−27.9	1.2	−0.1	0.0	−0.1	0.0	0.0

[a] Sum of isolated ethene and P450. [b] Long-range complex; r_{C-O} = 3.720 (quartet) and r_{C-O} = 4.338 (doublet). [c] Estimated from geometry scan; see text for details. [d] In parentheses are values for CH_3S^- as an axial ligand. [e] Terminal CH_2 group.

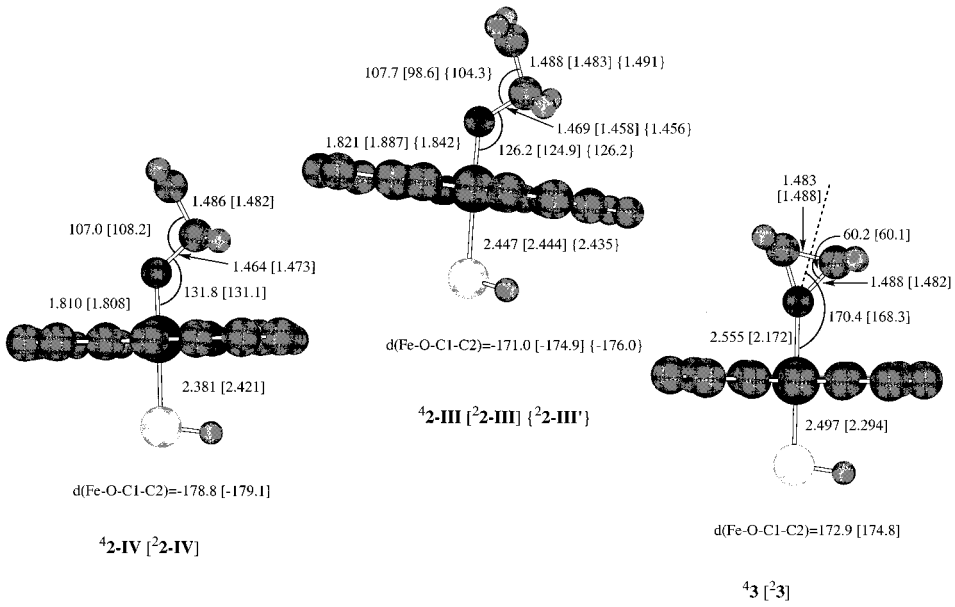

Figure 1. Optimized **2-IV**, **2-III**, and **3** structures in the quartet- and doublet spin states. Bond lengths are in Å and angles in degrees.

by Groves et al.[58] to occur en route to olefin epoxidation by ruthenium oxene.

Spin densities of the singly occupied π^*_{xz} and π^*_{yz} orbitals are spread over the iron and oxygen atoms, due to the fact that these orbitals represent the antibonding combinations of the π-(Fe−O) bond. The partially filled a_{2u} orbital gives spin densities distributed over the porphyrin and HS ligands.[30] Hence, the spin densities as written in Table 1 support the assignment of the orbital occupancy in Schemes 2−5 and thereby ascertain that the calculations converged to the proper electronic state. Population of the $\sigma^*(d_{z^2})$ orbital places spin densities on the iron and SH moieties as this orbital involves the Fe−S antibonding combinations. Notice, however, the singly occupied π^* orbitals in **1** are Fe−O antibonding with equal share of spin density on both the iron and oxygen units. In the **2-IV** radical complex, however, the spin densities are strongly polarized toward the iron atom.

3.3. Transition State for Radical Intermediate Formation (TS1). En route from the reactants (^{2,4}**1** + C_2H_4) to the radical intermediates **2-IV** and **2-III**, there occur two low-lying transition states ^{2,4}**TS1-IV** of the Fe^{IV} variety. These transition states were obtained using tight-step path following which established that they form contiguous energy curves from the reactant states ^{2,4}**1** + C_2H_4 to the intermediates ^{2,4}**2-IV**. These curves are shown in Figures 2 and 3.

Corresponding structures along with the transition vector modes of the imaginary frequencies are shown in Figure 4.

The major activation in the transition state is apparent in the elongation of the Fe−O and C═C bonds relative to the reactants (**1** + C_2H_4).[30] In contrast, the Fe−S bond is shortened and mitigates thereby the barrier height.[30] This is a simple manifestation of the "push effect" of the thiolate ligand, and was originally invoked for facilitating the heterolytic cleavage of the FeO−OH bond.[2,5] With these structures of **TS1**, we are unable to assess the steric differentiation that would exist between *cis*- and *trans*-olefins.[50] The ethene as a whole seems to keep away from the porphyrin plane.

The electromeric Fe^{III} transition states are higher-lying. As such, their characterization and path-following is not a simple matter. They tend to converge to the lower-lying ^{2,4}**TS1-IV** species. Nevertheless, it was deemed necessary to have at least an estimate of the energetics and behavior of these ^{2,4}**TS1-III** species. This can be done by starting with ^{2,4}**TS1-IV** swapping electrons in appropriate orbitals to generate the **TS1-III** electronic configuration and subsequently proceeding with geometry optimization (and transition-state search). The resulting structures are assembled in Figure 5 along with their energies relative to that of the reactant states (^{2,4}**1** + C_2H_4).

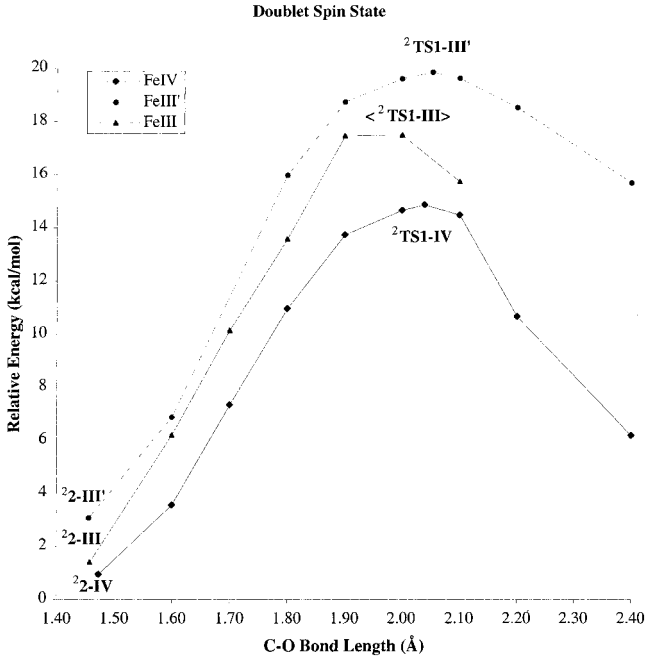

Figure 2. Potential energy scan starting at the radical complexes ^{2}**2-III′**, ^{2}**2-III**, and ^{2}**2-IV** in the direction of ^{2}**1**. Each point represents a full optimization with a given C−O bond distance. <^{2}**TS1-III**> is a higher-order saddle point.

The first species ^{2}**TS1-III′** is a true saddle point (imaginary frequency *i* 199 cm^{-1}) that correlates in the forward direction to the intermediate ^{2}**2-III′**. In the reverse direction it correlates with an excited state of the reactant in which the two π^* electrons of **1** are singlet-paired (see Figure 2). A lower-lying doublet species is indicated in Figure 5 as <^{2}**TS1-III**>, where

(58) Groves, J. T.; Ahn, K.-H.; Quinn, R. *J. Am. Chem. Soc.* **1988**, *110*, 4217.

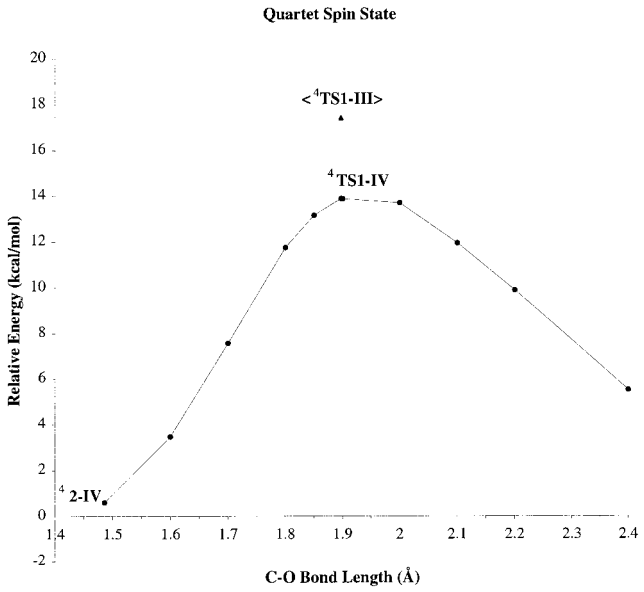

Figure 3. Potential energy scan starting at the quartet radical complexes in the direction of ^{4}**1**. Each point represents a full optimization with fixed C−O bond distance. <^{4}**TS1-III**> is not a true saddle point.

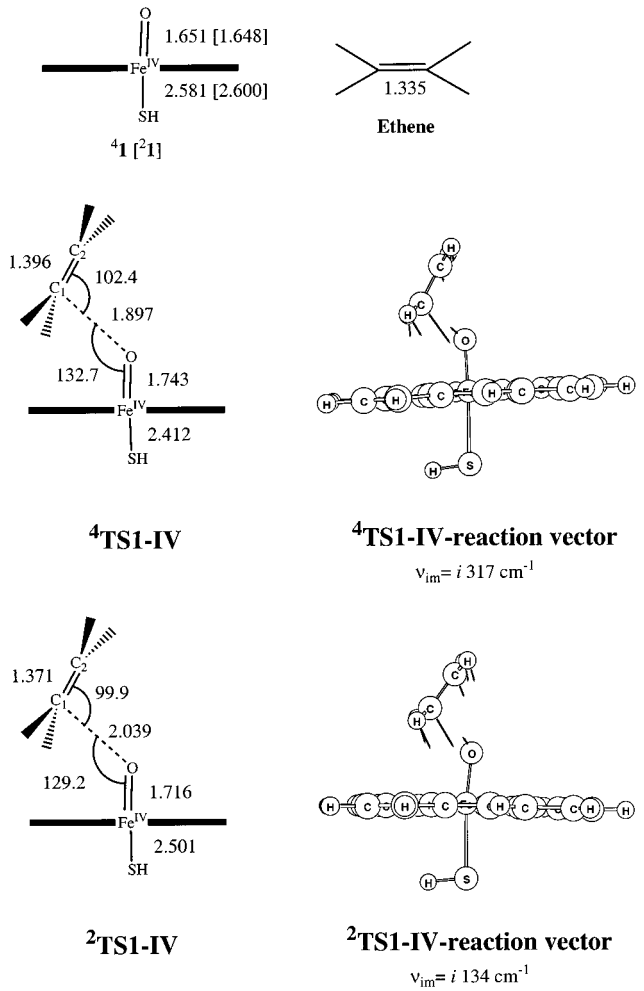

Figure 4. Optimized geometries of ^{2,4}**1**, ethene, ^{4}**TS1-IV**, and ^{2}**TS1-IV**. Bond distances are in Å and angles in degrees. The reaction vectors and the imaginary frequencies of ^{2,4}**TS1-IV** are shown.

the triangular brackets indicate that it is a higher-order saddle point (two imaginary frequencies). This species correlates to the intermediate structure ^{2}**2-III** in the forward direction. In the reverse direction, the <^{2}**TS1-III**> species converges to the ground state of ^{2}**1**. Similarly, <^{4}**TS1-III**> possesses three negative eigenvalues in the Hessian. Many attempts to follow it ended in its convergence to ^{4}**TS1-IV**. We failed to connect ^{4}**TS1-III** to ^{4}**2-III**. Starting with ^{4}**2-III** we always ended on ^{4}**TS1-IV**.

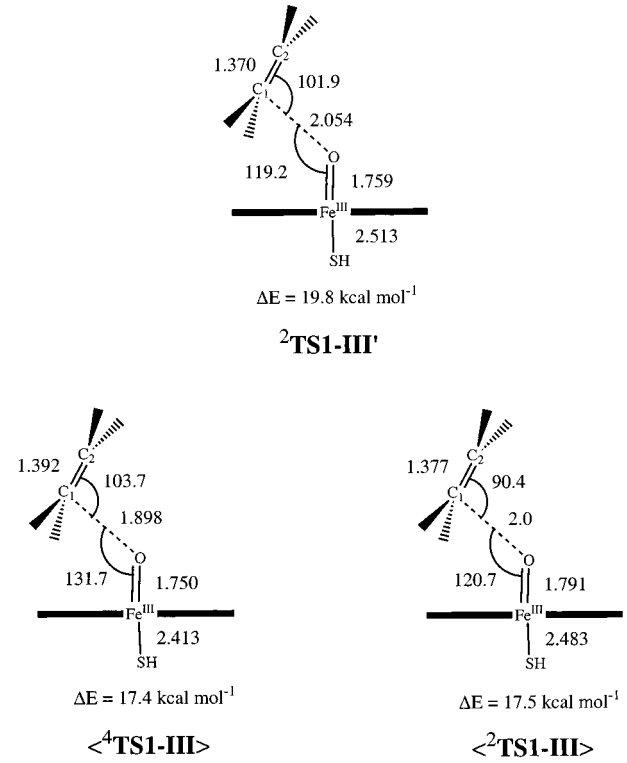

Figure 5. Geometries of ^{2}**TS1-III′**, <^{2}**TS1-III**>, and <^{4}**TS1-III**>. Energies are relative to ^{4}**1** + C_2H_4.

An interesting feature of all **TS1** species is their involvement of charge transfer from the olefin moiety to the ferryl oxene. The degree of charge transfer is 0.2 e^- in ^{4}**TS1-IV** and 0.3 e^- in ^{2}**TS1-IV** as shown in drawings **a** and **b** in Scheme 6. An insight into the electronic structure of **TS1** can be gained from the spin density data in Table 1. The quartet spin density is more reliable than the doublet's due to the single determinant nature of the Kohn−Sham wave function. The spin density distribution of ^{4}**TS1**, depicted in drawing **c**, shows that the carbon site of attack (C_α) bears a negative spin density and the two flanking groups (C_β and O) have positive spin densities. A similar feature characterizes the C−H activation transition state.[30] This feature is a mark of 3-electron/3-center delocalization and is typical to radical attack transition states.[30] Thus, **TS1** can be viewed as a radical attack of one of the π^*(Fe−O) orbitals on the π(C═C) bond. This description is in harmony with the stereoelectronic reasoning of Groves and Nemo[50] about the role for the π^*(Fe−O)/π^*(C═C) overlap in the transition state.

On the basis of the low-lying transition states, ^{2,4}**TS1-IV**, there are two competitive doublet- and quartet paths leading to the radical intermediates, ^{2,4}**2**. Furthermore, all of the intermediates ^{2,4}**2** are packed within 2.6 kcal mol^{-1} and are 0.6−3.2 kcal mol^{-1} higher than the reactant state. Thus, the bond-activation step of the oxidation is virtually thermoneutral for both reactive spin states.

Attempts to change the guess wave function of the radical complex **2** to a carbocationic species $PorFe^{III}OCH_2CH_2^+$, always ended back in the radical species **2**. Clearly, for the bare system, the carbocationic form is much higher in energy relative to the radical form. For radical centers with ionization energies of ∼8

Scheme 6

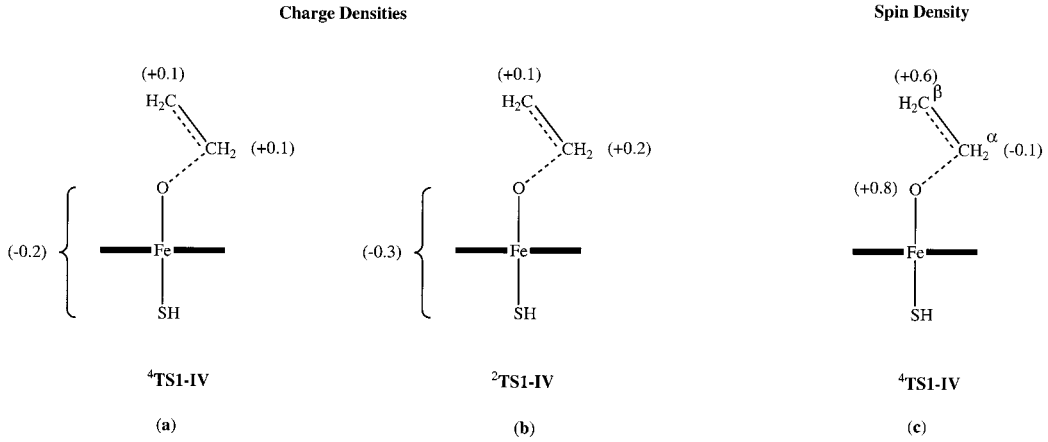

eV, the energy difference can be roughly estimated as >40 kcal mol^{-1}. This may be too large to be compensated for by solvation. For such radical centers, the carbocationic species, PorFe^{III}OCH$_2$CH$_2^+$, will be higher-lying than the corresponding radical (**2**) PorFeOCH$_2$CH$_2^\bullet$.

3.4. Transition State for Epoxide Complex Formation (TS2). The transition state which separates the radical intermediate (**2**) from the epoxide complex (**3**) is designated **TS2**. The energy- and spin density data are tabulated in Table 1. Figure 6 shows the intermediate complexes and their corresponding transition states for ring-closure. On the quartet potential energy surface a small barrier of 2.3 kcal mol^{-1} with respect to ^{4}**2-IV** leads to the product complex ^{4}**3**. A frequency analysis of ^{4}**TS2-IV** gave an imaginary frequency of *i*404 cm^{-1}, and a pictorial representation of this vibrational mode is given in Figure 6. The reaction vector corresponds to a motion that leads to ring-closure of the epoxide unit. In the transition state, the spin density (Table 1) on the terminal CH_2 group has reduced to 0.6. At the same time the spin density on the SH group is enhanced to 0.3, and the spin density on iron increases to 2.3. These spin densities are between those calculated for ^{4}**2-IV** and ^{4}**3**. Along the reaction pathway, the spin density on iron increases gradually from 1.0 (^{4}**1**) → 1.3 (^{4}**TS1**) → 1.9 (^{4}**2-IV**) → 2.3 (^{4}**TS2-IV**) → 2.6 (^{4}**3**), thus reflecting the changes in the electronic structure discussed in Schemes 2−5. The second transition state for ring-closure, ^{4}**TS2-III** is higher in energy and differs from ^{4}**TS2-IV** in its geometry. Although both transition states exhibit Fe−S and Fe−O bond lengthening, which account for the activation barrier due to the occupation of the d_{z^2} (σ^*) orbital, ^{4}**TS2-III** is not fully characterized as explained below.

The geometry scan of the minimum energy reaction path between ^{4}**2-III** and ^{4}**3** is schematically depicted in Figure 7. Attempts to precisely locate the transition state at the Fe^{III} potential energy surface failed. Therefore, the optimized geometry (^{4}**TS2-III**) depicted in Figure 6 represents the highest point along the geometry scan. It may be anticipated that the "true" ^{4}**TS2-III** transition state is close in energy and geometry to this structure. As already noted, the barrier for conversion of ^{4}**2-IV** into ^{4}**3** (2.3 kcal mol^{-1}) is much lower than the corresponding

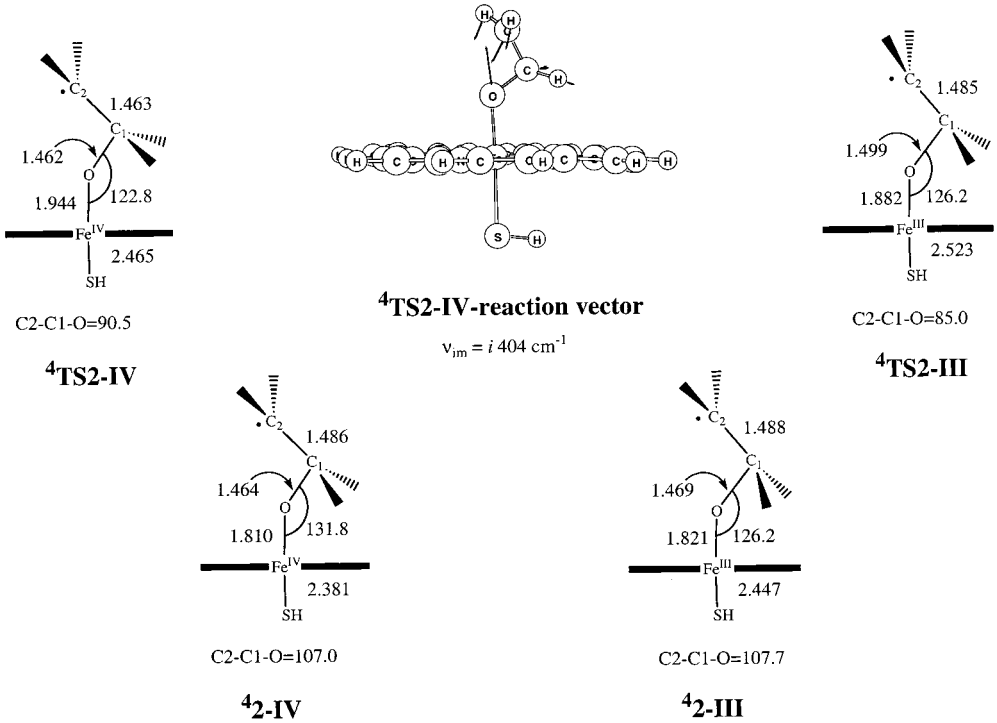

Figure 6. Optimized ^{4}**TS2-IV** geometry and corresponding reaction vector. Structure ^{4}**TS2-III** has been obtained with a fixed C−C−O angle of 85.0°, see text for explanation. Shown also are the intermediates ^{4}**2-IV** and ^{4}**2-III**. Bond distances are in Å and angles in degrees.

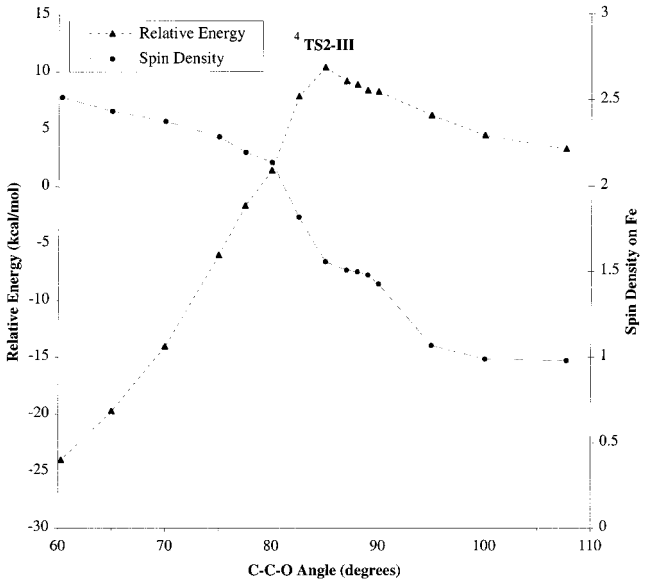

Figure 7. Relative energy and iron spin densities for the geometry scan starting at ^{4}**2-III** toward ^{4}**3**.

barrier (7.2 kcal mol^{-1}) on the Fe^{III} surface. This is mainly due to a double excitation that is necessary for the ^{4}**2-III** isomer to become ^{4}**3**, as opposed to a single excitation from the C• orbital in ^{4}**2-IV** to the $\sigma^*(d_{z^2})$ orbital in ^{4}**3** which is achieved via ^{4}**TS2-IV**. Thus, the double excitation of ^{4}**2-III** involves, apart from the C• $\rightarrow \sigma^*(d_{z^2})$ excitation of an alpha spin electron, also an excitation of a beta spin electron from the π^*_{xz} to the a_{2u} orbital, at a phase where the latter orbital is still of higher energy (recall discussion of Schemes 3 and 5). The same trends were observed in the rebound step of the hydroxylation mechanism, where a smaller rebound barrier was calculated for the iron(III)-hydroxo intermediate compared with the iron(IV)-hydroxo intermediate.[30]

Our previous hydroxylation studies[30] showed that on the doublet potential energy surface the rebound barrier is vanishingly small. The second step in the doublet-state epoxidation process shows much analogy with the hydroxylation mechanism. A geometry scan along the C−C−O angle on the doublet potential energy surface starting at ^{2}**2-III**, ^{2}**2-III′** and ^{2}**2-IV** has been performed and is schematically depicted in Figure 8. The product complex ^{2}**3** has an iron atom in oxidation state III and can be formed directly from the ^{2}**2-III** and ^{2}**2-III′** intermediate complexes. The scan of these states shows that the barrier for going from ^{2}**2-III** or ^{2}**2-III′** to ^{2}**3** is smaller than 0.3 kcal mol^{-1}. The scan which started at ^{2}**2-IV** crosses the ^{2}**2-III** (^{2}**2-III′**) surfaces, around a C−C−O angle of 95°, and the height of the crossing point is again equal to or less than 0.3 kcal mol^{-1} (see Figure 8).

3.5. Internal Rotation in the 2-Intermediate. To check the possibility of *cis*−*trans* isomerization[3,21] in our model system we have run a potential energy scan of the rotation about the C−C bond in the radical complex at the quartet spin state, using the RODFT method. The quartet radical complex (^{4}**2-IV**) is in a potential minimum between two transition states, ^{4}**TS1-IV** and ^{4}**TS2-IV**, with barrier heights of 13.3 and 2.3 kcal mol^{-1}, respectively. The terminal CH_2 group of ^{4}**2-IV** was rotated 360° stepwise by changing the dihedral angle (H1−C−C−O) from 82.8° to 442.8°, while the dihedral angle (H2−C−C−H1) stayed constant. All other geometrical parameters were fixed. Energies relative to the starting point have been calculated, and the results are schematically depicted in Figure 9. While Figure 9 results from stepwise single-point calculations, still the maximum

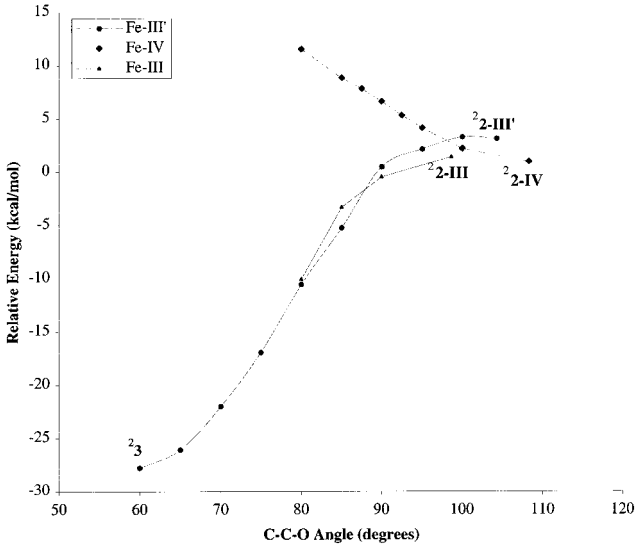

Figure 8. Relative energies of the geometry scans starting at ^{2}**2-III**, ^{2}**2-III′**, and ^{2}**2-IV** in the direction of ^{2}**3**. Note that both ^{2}**2-III** and ^{2}**2-III′** correlate to ^{2}**3**.

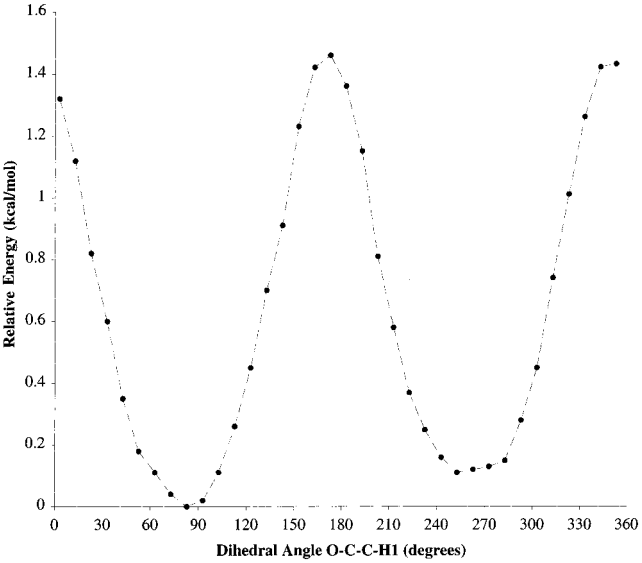

Figure 9. Relative energies of internal rotation of the terminal CH_2 group. The energies are relative to the optimized ^{4}**2-IV** geometry, which has a dihedral of 82.8°. Each point represents a single-point calculation.

barrier for internal rotation, 1.4 kcal mol^{-1}, is lower than the barriers for reaching either of the two transition states (^{4}**TS1-IV** and ^{4}**TS2-IV**). Consequently, internal rotation of the terminal methylene group is feasible and might well happen during the lifetime of the radical intermediate. With the small difference between barrier heights for rotation (1.4 kcal mol^{-1}) and ^{4}**TS2-IV** (2.3 kcal mol^{-1}) quite small changes in experimental conditions (solvent, temperature, ligands) could easily have a large effect on the amount of isomerization. Since this rotational barrier is larger than the tiny barriers in the doublet state, ^{2}**2-IV** or ^{2}**2-III**, the doublet radical complex will not exhibit *cis*−*trans* isomerization. Rather as we already concluded, the doublet mechanism will feature an effectively concerted epoxidation.

4. Discussion

The details of the potential energy profile for ethene epoxidation by a model P450 iron oxene species (**1**) are assembled in Scheme 7. This information and the charge-transfer character

Scheme 7

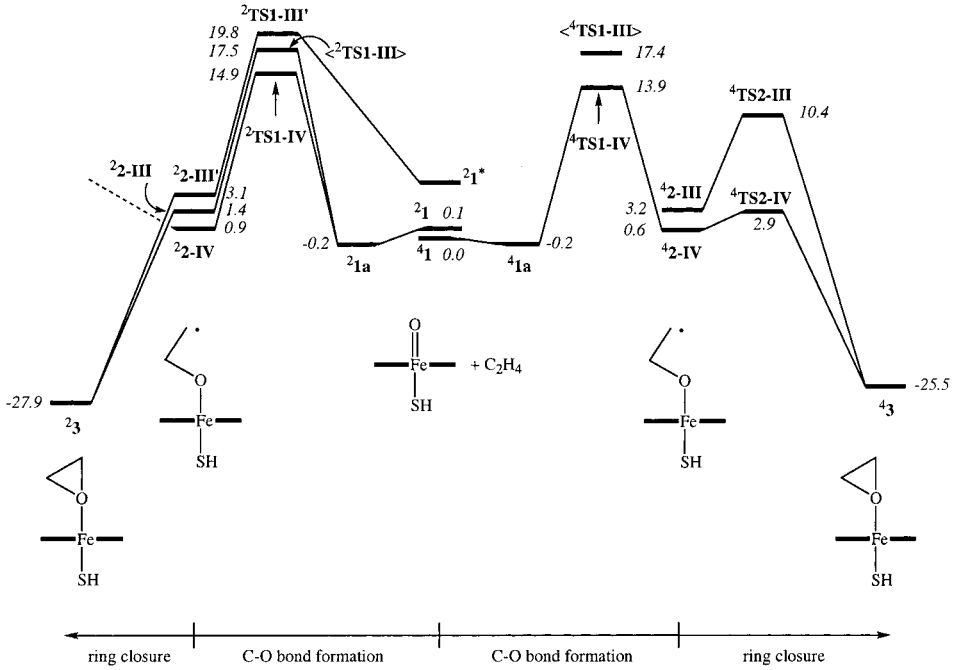

of **TS1** in Scheme 6 form the basis for the discussion. Starting from the center of Scheme 7, the quartet state profile stretches to the right while the doublet profile stretches to the left. In both cases the initial step of the reaction involves formation of a carbon−oxygen bond that leads to a radical intermediate, **2**. To simplify the arguments, we disregard ^{2,4}**TS1-III**, due to their higher energy compared with the ^{2,4}**TS1-IV** transition states and since they are not true saddle points. With the simplification, the quartet and doublet profiles are extremely close in energy, almost throughout the process. Consequently, the epoxidation process involves two-state-reactivity (TSR) in which the product information involves the interplay of the patterns typical to the two states.

Further complexity is conferred by the coexistence of Fe^{III} and Fe^{IV} states for the radical intermediate. Thus, in the second phase of the process, the number of states that may participate in the ring-closure is increased to five. In the in-vacuum conditions of the calculations, the **2-IV** state is of lower energy. However, since the **2-III** state possesses a porphyrin cation radical, it is more polarizable and is expected to be stabilized in excess relative to the **2-IV** states. Indeed, our previous calculation of the corresponding iron-hydroxo species,[43] show that a polarizing medium stabilizes the Fe^{III} state by ∼5 kcal mol^{-1} better than the IV-state.[59] This would make the two radical intermediates competitive, and their interconversion will be controlled by intrinsic and solvation reorganization factors involved in the electron shift between the a_{2u} and the $\pi^*(d_{xz}, d_{yz})$ orbitals. This is similar to medium polarization effects in internal electron-transfer processes. We have no hard data to discuss this aspect (not possible with DFT computations), but if we make the reasonable assumption that the interconversion barriers are not larger than the computed energy gaps between **2-IV** and **2-III**, we expect then equilibration of the intermediate species. Assuming such an equilibration, the quartet-state bond-closure processes have sufficiently high barriers, higher than that for C−C internal rotation. *Consequently, the quartet intermediates ^{4}**2-IV** and ^{4}**2-III** will be sufficiently long-lived to undergo cis/trans isomerization*. In contrast, in the doublet state, the radical intermediates will have virtually no barriers since the ^{2}**2-IV** intermediate will cross over to the ^{2}**2-III** state and proceeds thereafter in a barrierless fashion to product. *It follows therefore, that the doublet-state mechanism will be effectively concerted*. Using radical clocks to determine the lifetime of the radical intermediate in such a two-state system will lead to too short lifetimes and occasionally to a false information.[30] Thus, the measured ultrashort radical lifetime[1,3,8e] which is used to discard the hypothesis of radical intermediacy, may originate in the TSR feature of the mechanism.

Another possible intermediate, which has been considered, is the carbocation species, $PorFe^{(III)}-O-CH_2-CH_2^+$.[1,3,8e] As we have discussed in the Results section, this species is too high for the bare system. For the P450 species (that is not a very good electron acceptor) and for radical centers with ionization energies of ∼8 eV, solvation (or interaction with the polarizing groups of the protein pocket) will not be sufficient to make these $PorFe^{(III)}-O-CH_2-CH_2^+$ species competitive with the radical intermediate. However, when the porphyrin is polyhalogenated, when the axial ligand is not a good internal donor or is altogether missing, and when the radical center is highly substituted with gas-phase ionization energy of <7 eV, a carbocation intermediate is plausible. This intermediate will occur only on the doublet manifold.

The radical intermediates in Scheme 7 are expected to dominate the chemistry of P450 epoxidation of olefins with moderate donor capability. With this mechanistic scheme, the extent of *cis*/*trans* isomerization will depend to a large extent on the spin state crossover, which controls the rate of passage from the doublet- to the quartet state and on the relative heights of ^{4}**TS1-IV** and ^{2}**TS1-IV**. The present calculation with the simplified models shows that the quartet barrier is slightly lower. However, as shown by us recently[46] larger basis sets and especially polarizing media tend to prefer the doublet state. In such a case and if spin crossover, en route to **TS1**, is not fast on the reaction time scale, there will be a preference for the doublet process and a high degree of stereochemical retention.[1]

(59) The relative stabilization energy in ref 43 of 13 kcal mol^{-1} did not take into account the energy cost of polarizing the bare molecule. With this term, the relative stabilization energy is 5 kcal mol^{-1} in favor of the Fe^{III} state. Such a value will make **2-III** slightly more stable.

Spin-crossover can occur en route to **TS1**[44] or at the stage of the intermediate, **2**. The ^{2,4}**2-III** intermediates can undergo scrambling since they can mix indirectly with the analogous ^{2,4}**2-III$_{xz}$** species in which the d-orbital occupation is $d_{xz}^1 d_{yz}^2$ instead of $d_{xz}^2 d_{yz}^1$ for ^{2,4}**2-III** (Scheme 3).[43] This mixing will result in a significant iron-centered spin−orbit coupling interaction and will induce efficient quartet−doublet crossovers. Since the doublet intermediate transforms to an epoxide complex in a barrierless fashion, this spin-crossover will have a serious impact on the stereochemistry of the epoxidation. Clearly, these aspects of the reactivity require more sophisticated studies of the spin-crossover factors. However, such a full-scale calculation of the spin crossover dynamics along the entire path is still beyond the present means.

While our study is a very simplified modeling of a "real" epoxidation by P450, nevertheless its results make some links to experimental trends. The first and foremost link is the similarity between the computed mechanism and the experimentally described one.[21,29] Especially striking is the similarity to the recently described mechanistic scheme by Gross et al.[29] where the intermediates **2-III** and **2-IV** play a major role. Thus, our study vindicates the stepwise mechanism,[21,29] albeit in a two-spin-state scenario.

The stepwise mechanism involving some kind of intermediate has gained support from various studies.[1,3,8e] Gross et al.[29] who support a radical mechanism have shown that the axial ligand has a pronounced effect on the lifetime of the radical. With ligands which stabilize the Fe^{III} form, presumably analogous to ^{4}**2-III** in our study, the radical was sufficiently long-lived to afford spectroscopic characterization. On the other hand, with ligands which stabilize the radical form **2-IV** (presumably ^{4}**2-IV**), the radical intermediate did not accumulate.[29] Accumulation of the radical in the ^{4}**2-III** state due to the high barrier to ring-closure (See Scheme 7) was invoked[29] to explain the formation of an aldehyde byproduct due to 1,2-hydrogen shift followed by Fe−O bond cleavage.[21,29,60] Furthermore, early on, Groves and Watanabe[61] have shown that an intermediate is formed reversibly and can thereby return to its precursor Compound I (analogous to **1**) under certain conditions. While in the original paper, this was considered to be a charge-transfer complex, the Groves−Watanabe intermediate might well be ^{4}**2-III**.

A related aspect is the role of the thiolate ligand. Higuchi, Nagano et al.[62] have demonstrated on model complexes that the thiolate ligand is necessary to mimic a P450-like reactivity. This was attributed to the internal donor property of the thiolate which tends to disfavor an Fe^{III} situation.[12,63,64] In terms of Scheme 7, this is equivalent to a fluxional behavior of **2** between the forms ^{4}**2-III** and ^{4}**2-IV**, and a tendency of good donor ligands to prefer the latter form relative to lesser donor ligands. This may account for the fact that the thiolate ligand affords a high degree of stereospecificity,[3,8b,29] in line with the small barrier computed for the ring-closure of ^{4}**2-IV** (Scheme 7). On the other hand, with non-thiolate ligands the ^{4}**2-III** state is stabilized, and with its high barrier for ring-closure will give rise to a high degree of *cis*−*trans* isomerization and aldehyde production via 1,2-hydrogen shift in the radical moiety followed by Fe−O cleavage.[21,29,60] Traditionally, these kinds of differences have been analyzed in terms of two oxidants. Our investigations indicate that the complexity of the results can be accommodated with a single oxidant, a Compound I type.

Another trend can be deduced from the charge-transfer information in ^{2,4}**TS1-IV**; shown in drawings **a** and **b** in Scheme 6 above. Thus, it is expected that as the olefin becomes a better electron donor and the ferryl oxene species a better acceptor, this will be attended by a decrease of the barrier for bond insertion (**TS1** lowering). Such trends have been noted indeed by Groves et al.[21] and Gross et al.[29] and are reported for chromium oxene by Ostovic and Bruice.[1] We might further expect that the doublet state will benefit more from the improvement of the donor−acceptor relationship (see **a** versus **b** in Scheme 6 above). If this is indeed the case, better donor olefins will yield more stereospecific epoxidations. These are some of the possible articulations of the computed epoxidation mechanism (Scheme 7). Finding reliable probes for the two-state nature of the mechanism can make further progress.

5. Conclusions and Summary

The reaction of iron porphyrin (**1**) with ethene to yield an epoxide has been studied by computational methods. The reaction can be explained by two-state reactivity (TSR) of competing quartet- and doublet spin states. In addition, two oxidation states are involved in the reaction process: one with an Fe^{IV} oxidation state (neutral porphyrin system) and one whereby the iron has an oxidation state of Fe^{III} (cation radical porphyrin ring). The barrier heights show that the overall reaction on the quartet surface follows a stepwise mechanism via a radical intermediate (**2**). In both the quartet- and doublet spin states the Fe-III and Fe-IV electromers of **2** are reached via ^{2,4}**TS1**, of 13.9 kcal mol^{-1} and 14.9 kcal mol^{-1} above the reactants. Subsequently, on the doublet surface a tiny barrier (<0.3 kcal mol^{-1}) leads to internal conversion into the product epoxide complex (^{2}**3**). In contrast, the ^{4}**2-III** and ^{4}**2-IV** intermediates have significant barriers for ring-closure of 7.2 and 2.3 kcal mol^{-1}, respectively (see Scheme 7 for details). Thus, a longer lifetime is expected for the ^{4}**2-III** radical intermediate. In contrast, the much smaller ring-closure barrier on the doublet surface indicates that the doublet-state epoxidation could well be effectively concerted. These mechanistic features resemble our previous findings for alkane-hydroxylation.[30]

Acknowledgment. The research at the Hebrew University is supported in part by an ISF grant to S.S. and in part by the Robert Szold Fund and the Ministry of Science, Culture and Sport. F.O. thanks the European Union for a Marie Curie Fellowship.

Supporting Information Available: (a) Two Tables with absolute energies, group charges, and spin densities of optimized geometries and (b) a Figure of spin densities and associated discussion for ^{4}**TS1-IV** (PDF). This material is available free of charge via the Internet at http://pubs.acs.org.

JA003544+

(60) The 1,2-shift appears more likely for a carbocation intermediate. But in the complex, **2**, such a rearrangement in the radical moiety may have a different barrier than for the free radical. Such a calculation is currently attempted.

(61) Groves, J. T.; Watanabe, Y. *J. Am. Chem. Soc.* **1986**, *108*, 507.

(62) Urano, Y.; Higuchi, T.; Hirobe, M.; Nagano, T. *J. Am. Chem. Soc.* **1997**, *119*, 12008.

(63) Weiss, R.; Mandon, D.; Wolter, T.; Trautwein, A. X.; Müther, M.; Bill, E.; Gold, A.; Jayaraj, K.; Terner, J. *J. Bioinorg. Chem.* **1996**, *1*, 377.

(64) Champion, P. M. *J. Am. Chem. Soc.* **1989**, *111*, 3433.